HHS Public Access

Author manuscript

Neurobiol Dis. Author manuscript; available in PMC 2021 April 29.

Published in final edited form as:

Neurobiol Dis. 2020 August ; 142: 104949. doi:10.1016/j.nbd.2020.104949.

Prolonged prophylactic effects of gabapentin on status epilepticus-induced neocortical injury

Maria-Belen Perez-Ramirez, **Feng Gu**, **David A. Prince***

Department of Neurology and Neurological Sciences, Stanford University School of Medicine, Stanford, CA 94305, USA

Abstract

Long-term consequences of status epilepticus (SE) occur in a significant proportion of those who survive the acute episode. We developed an in vivo model of acute focal neocortical SE (FSE) to study long-term effects on local cortical structure and function and potential strategies to mitigate adverse consequences of SE. An acute 2 h episode of FSE was induced in anesthetized mice by epidural application of gabazine +4-aminopyridine over sensorimotor neocortex. Ten and 30 days later, the morphological and functional consequences of this single episode of FSE were studied using immunocytochemical and electrophysiological techniques. Results, focused on cortical layer V, showed astrogliosis, microgliosis, decreased neuronal density, and increased excitatory synapses, along with increased immunoreactivity for thrombospondin 2 (TSP2) and α2δ-1 proteins. In addition, neocortical slices, obtained from the area of prior focal seizure activity, showed abnormal epileptiform burst discharges along with increases in the frequency of miniature and spontaneous excitatory postsynaptic currents in layer V pyramidal cells, together with decreases in both parvalbumin immunoreactivity (PV-IR) and the frequency of miniature inhibitory postsynaptic currents in layer V pyramidal cells. Treatment with an approved drug, gabapentin (GBP) (ip 100 mg/kg/day 3 × /day for 7 days following the FSE episode), prevented the gliosis, the enhanced TSP2- and α2δ-1- IR and the increased excitatory synaptic density in the affected neocortex. This model provides an approach for assessing adverse effects of FSE on neocortical structure and function and potential prophylactic treatments.

Keywords

Focal neocortical SE; Epileptogenesis; Neuronal injury; Gliosis; Aberrant hyperexcitability; SE prophylaxis

*Corresponding author. daprince@stanford.edu (D.A. Prince).

Authors contributions

BP-R and FG performed the experiments; BP-R and DAP wrote and revised the manuscript; FG revised the manuscript; BP-R, FG and DAP generated the figures.

Declaration of Competing Interest

The authors declare no competing financial interest.

Supplementary data to this article can be found online at https://doi.org/10.1016/j.nbd.2020.104949.

1. Introduction

Epilepsy is among the most common brain disorders affecting individuals of all ages. Episodes of unprovoked seizures lasting more than 5 min are defined as status epilepticus (SE) and can occur in patients with or without a prior diagnosis of epilepsy (DeLorenzo et al., 1995; Hesdorffer et al., 1998). The pathophysiological and anatomical consequences of a single episode of FSE are not fully understood. However, it is known that SE increases the probability for subsequent unprovoked seizures in humans and animal models (Holtkamp et al., 2005; Santamarina et al., 2015). For example, there is evidence that prolonged febrile seizures in children may result in hippocampal/limbic system epilepsy (Feng and Chen, 2016; Patterson et al., 2014). Therapy for SE has focused predominantly on arresting ongoing seizures with antiepileptic drugs. To date there is no available therapy to prevent epileptogenesis or other co-morbidities following SE.

In most experiments dealing with consequences of SE in partial (focal) or generalized epilepsy models, SE is induced by systemic drug administration or local injection of convulsants into limbic brain structures (temporal lobe epilepsy models). Some of these studies have shown that SE induced in limbic system structures can result in significant abnormalities in the neocortex (Silva et al., 2005; Teskey et al., 1999). Nonetheless, there is a paucity of data relevant to the consequences of a single episode of FSE. The characteristics, and course of epileptiform seizures induced by topical application of convulsant drugs to neocortical areas have been described (Ayala et al., 1970; Baracskay et al., 2008; Collins and Olney, 1982; Yang and Rothman, 2001). However, data regarding the chronic consequences of an acute episode of FSE are incomplete. In particular, it is important to know whether acute, prolonged focal neocortical epileptiform activity can induce alterations that would increase chronic susceptibility to subsequent seizures, and whether there might be therapeutic interventions that would limit detrimental effects of FSE. Here we show that long-lasting structural and functional abnormalities in excitatory and inhibitory neocortical networks occur after neocortical FSE, and that an antiepileptogenic drug, GBP, given after FSE, can limit FSE-induced gliosis, increases in synaptogenic proteins TSP2 and a2d-1 and development of new excitatory connectivity.

2. Materials and methods

All experiments were performed according to the National Institutes of Health guide for the care and use of Laboratory animals and all protocols were approved by the Stanford Institutional Animal Care and Use Committee.

2.1. Focal status epilepticus induction

The time line for experiments is shown in Fig. 1A. Focal neocortical SE was induced in anesthetized (Ketamine/Xylazine 80/8 mg/kg) adult (P 80–120) male and female FVB mice by unilateral application of a pledget centered 3 mm lateral to the midline and 1 mm posterior to bregma (plate 40, bregma-1.06, in (Franklin and Paxinos, 1997)). EEG epileptiform activity and associated contralateral partial seizures were monitored for two hours. The pledget was then removed and the cortex washed with sterile saline (0.9% NaCl). To further limit the seizure activity, diazepam was administered intraperitoneally (i.p. 5–10

mg/kg). Mice were allowed to recover for 10 and 30d prior to immunocytochemistry (ICC) or electrophysiological in vitro slice experiments. An age-matched naïve control group was treated identically, except that the dura was exposed to a saline moistened pledget without convulsant drugs.

2.2. Immunocytochemistry

Either 10 or 30d after FSE, SE-induced and control naïve mice were deeply anesthetized with fatal plus, perfused intracardially with 4% paraformaldehyde and brains post-fixed overnight at 4 °C followed by cryoprotection. 40 μm sections were obtained with a sliding microtome (Microm, HM 400) and rinsed in PBS followed by incubation with primary antibodies at 4 °C for 12–48 h. To estimate the excitatory synapse number, dual immunocytochemistry (ICC) was used with antibodies for vesicular glutamate transporter VGLUT-1(SySy, Gottingen, Germany 1:1000) and the postsynaptic marker PSD95 (In Vitrogen Illinois, USA 1:500) (Takahashi et al., 2016).To estimate gliosis, we used an antibody against glial fibrillary acidic protein (GFAP, Millipore, Massachusetts, USA, monoclonal 1:1000) (Li et al., 2012). Neurofilament immunoreactivity was examined with Neurofilament H-171111 (SySy, Gottingen, Germany 1:500). Monoclonal antibodies were used to assess the expression of thrombospondins (TSPs; BD Transduction Labs, California USA, dilution 1:200) and the Ca^{++} channel subunit α2δ-1 (Sigma, Missouri, USA, 1:300) (Eroglu et al., 2009; Li et al., 2012). Neuronal cell loss was evaluated using counts of immunoreactive neurons for the neuronal specific nuclear protein (NeuN, Millipore, Massachusetts, USA, 1:1000, see below) and for parvalbumin (PV, Synaptic Systems, Germany, 1:500). Immunofluorescence was visualized with laser scanning confocal microscopy (LSM Zeiss 880 inverted confocal Airyscan GaAsP detector). Image stacks were obtained with 0.25 μm separation in the z-axis at 63 × and 40 ×. Confocal images were analyzed by measuring the immunoreactive pixel area for a given antibody within the ROI, using Cell profiler software (Gu et al., 2017). Colocalized pixel area measurements for VGLUT1 and PSD95 were made within 40 × 40μm^2 areas of neocortical layer V and pixel areas for TSP2, α2δ-1, and GFAP were obtained in 200×200μm^2 single plane sections of neocortical layer V at 40×. Results are reported as the IR percentage area for a 200×200μm^2 grid (TSP2, α2δ-1 and GFAP) or 40×40μm^2 grid (VGLUT1/PSD95).

2.3. Neuronal cell counts

Neuronal cell counts were made as previously reported, (Gu et al., 2017). In short, the number of neurons was assessed in a region of interest (ROI) within the convulsant drug application area, 1 mm away from midline. The ROI corresponded to a 420 μm-wide cortical column extending from the pial surface to the junction between layer VI and the white matter. Counts of NeuN labeled and parvalbumin immunoreactive (PV-IR) neurons were obtained from non-overlapping 40 μm confocal sections and analyzed using iLastik and Cell Profiler programs (Gu et al., 2017). Values are reported as the mean number of neurons per ROI ± standard error of the mean.

2.4. Slice preparation

Animals were deeply anesthetized with sodium pentobarbital (55 mg/kg ip). Brains were rapidly removed and placed in ice-cold (4 °C) sucrose artificial cerebrospinal fluid cutting

solution (sACSF) containing (in mM): 234 sucrose, 26 $NaHCO_3$, 11 glucose, 10 $MgSO_4$, 2.5 KCl, 1.25 NaH_2PO_4, and 0.5 $CaCl_2$, gassed with 95% O_2/5% CO_2. The neocortex was blocked and mounted on a vibratome stage (VT 1200, Leica). Coronal brain slices (400 or 250 μm) containing the sensorimotor cortex from controls and the same area in post-FSE mice were cut in oxygenated sACSF and immediately transferred to an incubation chamber filled with oxygenated ACSF containing (in mM): 2.5 KCl, 126 NaCl, 1.25 NaH_2PO_4, 2 $MgSO_4$, 2 CaCl, 26 $NaHCO_3$, 10 glucose; osmolarity 290–300 mOsm, pH 7.4 saturated with 95% O_2/5% CO_2. Slices were incubated at 30 °C for 1 h and then at room temperature until they were transferred one by one to the interface recording chamber and maintained at 30–32 °C for the local field potential recordings.

2.5. Local field potential recordings

Coronal brain slices (400 μm) were visualized with a dissecting microscope and partially submerged and superfused continuously (~3 ml/min) with ACSF containing in mM: 5 KCl, 126 NaCl, 1.25 NaH_2PO_4, 2 $MgSO_4$, 2 CaCl, 26 $NaHCO_3$, 10 glucose, 100 μM glutamine; osmolarity 290–300 mOsm, pH 7.4 equilibrated with 95% O_2, 5% CO_2 and maintained at 30–32 °C. Local field potentials (LFPs) were recorded from neocortical layer V with borosilicate glass micropipettes (2–3 MΩ impedance) filled with ACSF. A concentric bipolar tungsten electrode (FHC), with inner pole diameter 25 μm, was placed at the layer VI/white matter junction, on column with the recording electrode. Series of 0.1 Hz stimuli consisting of single 100 μs square-wave current pulses were delivered at increasing intensities (0.75–3 μA) through a stimulation isolation unit. Additionally, continuous 3 min recordings were made to capture occasional spontaneous epileptiform events. Epileptiform responses consisting of variable latency bursts of all-or none polyphasic events usually lasting ≥100 milliseconds were evoked in FSE cortex, but rarely in controls (Graber and Prince, 2004).The minimum stimulus intensity needed to evoke 50% epileptiform responses and 50% failures was established as the threshold stimulus. Other briefer (< 100 ms) polyphasic LFPs were also evoked at low stimulation intensities (e.g. 0.8 μA 100 μs pulses) in post-FSE slices, but not in controls. To quantify the degree of hyperexcitability in field potential recordings, we used the “coastline bursting index” (Korn et al., 1987).

2.6. Patch clamp recordings

Single whole cell voltage clamp recordings were made from coronal brain slices (250 μm). Patch pipettes were pulled from borosilicate glass and had resistances of 4–6 MΩ when filled with internal solution containing in mM: 120 Kgluconate, 11 KCl, 1 MgCl, 1 CaCl, 10 HEPES, 1 EGTA, 3 ATP–Na, and 0.2 GTP. The osmolarity of the internal solution was adjusted to 280–290 mOsm and the pH to 7.3 with 1 M KOH. Cells were visualized using a water immersion lens (Achroplan 63 ×, 0.9 W, Carl Zeiss). Layer V_A pyramidal neurons were identified as large somata neurons with a single emerging apical dendrite oriented toward the pial surface. Voltage clamp recordings were obtained at −70 mV. Series resistance compensation (> 70%) was used to minimize the voltage error due to voltage drop across the electrode. Access resistance was monitored in voltage clamp from responses to small hyperpolarizing voltage pulses and data rejected for recordings where it fluctuated > 15%. Spontaneous excitatory postsynaptic currents (sEPSCs) were recorded for 3 min. Burst events resembling epileptiform discharges were present during the sEPSC recordings and

were excluded for the analysis of sEPSC frequency and amplitude. Miniature (m) EPSCs and inhibitory postsynaptic currents (mIPSCs) were recorded in the presence of 1 μM tetrodotoxin (TTX); mIPSCs were also recorded with Cs-gluconate in the internal solution at a holding potential of +20 mV. Recordings were obtained with a Multiclamp 700A amplifier and Clampex 10.2 software interfaced to a Digidata 1440A (Molecular Devices). EPSCs and IPSCs were identified and analyzed with MiniAnalysis (Synaptosoft).

2.7. EEG recordings

Before the application of the convulsant drugs, epidural electrodes were placed in 3 holes drilled over both hemispheres at sites between bregma and lambda and ~ 2 mm from the midline, marked by squares 1–3 in Fig. 1D. A reference electrode was implanted in the midline over the cerebellum (square number 4 in Fig. 1D). Electrodes were connected to an EEG preamplifier (VOUTn = 10 (VInn - VREF) and signals were filtered through a 500 Hz low pass filter. EEG signals were recorded, digitized and stored for later analysis (pCLAMP) without further filtering. EEG recording sessions began 10 min before drug placement (Fig. 1B) and were continuous for 2.1–3 h after convulsant drug application. Seizure onset began as regular interictal spikes that evolved over ~1 h to ictal activity (Fig. 1C, lead 3–4).

2.8. Statistical analysis

Data analysis and graphing was processed with Graph Pad Prism 7. Statistical analysis was performed using unpaired Mann-Whitney *U* test, Unpaired *t*-test or Kruskall-Wallis with Dunn's posthoc test with a $p < .05$. Comparisons were made between age-matched controls, FSE-induced + saline mice and GBP treated FSE mice. Data are expressed as mean ± standard error of the mean (S.E.M).

3. Results

3.1. Behavioral and focal electrographic status epilepticus

Focal SE was induced by unilateral application of a pledget soaked with 4AP and GABAzine (150 μM each) to the dura overlying the sensorimotor cortex. A total of 129 adult anesthetized mice had convulsant drug application and EEG recordings, of these, 43 were excluded from the results, including 8 animals that had generalized behavioral seizures with ipsilateral and contralateral electrographic ictal discharges, 3 animals that did not develop FSE, and 32 animals that died during recovery from the FSE. The remaining 86 animals recovered from the FSE and were used for electrophysiological and immunocytochemical experiments. Groups of 47 and 40 mice were studied 10d and 30d post-FSE, respectively. In the 10d group, 21 mice were used for immunocytochemical and 26 for electrophysiological experiments. In the 30d group, 17 mice were used for immunocytochemical and 23 for electrophysiological experiments.

Electrographic interictal discharges, consisting initially of single, high amplitude spikes, began 2 ± 1 min after the epidural drug application. Epileptiform EEG activity evolved over ~1 h into higher frequency polyspike bursts at the site of the convulsant drug application, associated with contralateral jerking (Fig. 1C). Behavioral seizures consisted of contralateral myoclonic hind-limb jerking starting 16 ± 9 min after the convulsant drug application.

Generalized seizures were detected in some animals as high amplitude and high frequency spikes in all recording electrodes along with behavioral bilateral jerking. Only animals with FSE without generalization were included in the present study. During ictal episodes, EEG recordings showed repetitive bursts of high amplitude, high frequency unilateral focal epileptiform activity in the area of convulsant drug application site (Fig. 1C). Mean spike frequency within bursts was 10 ± 3 Hz (Fig. 1C, E) that was projected at lower amplitude contralaterally and anterior to the pledget site (leads 1–4 and 2–4 of Fig. 1C). Two hours after the behavioral seizure activity began, the pledget was removed, the cortex washed with saline solution and diazepam (ip 5–10 mg/kg) given to stop the behavioral seizures. Diazepam completely suppressed behavioral seizures in 8 animals within 5 to 10 min, while contralateral behavioral jerking persisted in the other 78 mice for up to 2.5 h after the diazepam injection. EEG was not monitored beyond 2 h, so that the duration of subclinical continuing focal discharges could not be assessed.

3.2. Decreased neuronal density in the neocortex following status epilepticus

A group of 4 mice were perfused 10d after FSE induction and brains processed for cortical cell counts. Neuronal profiles were counted in NeuN immunoreacted tissue in single 420 μm wide confocal sections, extending through all cortical layers from the pial surface to the junction between layer VI and the white matter (Methods; Fig. 2A, B). A decrease in the density of NeuN labeled neurons was prominent in both supra- and infragranular lamina in cortex sections from the post-FSE mice (cf sections A and B of Fig. 2). Neuronal density was assessed by counting the total number of NeuN-IR neurons per ROI. Ten days after recovery from FSE, the density of the neuronal population was reduced by 43% (control 1706 ± 68 neurons per ROI, $n = 10$ sections from 4 animals; FSE 974 ± 164 neurons per ROI, $n = 7$ sections from 4 animals; $p = .002$ unpaired Mann-Whitney U test) (Fig. 2C). The total thickness of the cortex in the area of drug application was 802 ± 20 μm in 7 sections from 4 SE animals and 878 ± 31 μm in 10 sections from 4 controls (p=.02; unpaired Mann-Whitney U test), a 9% reduction in the FSE mice; e.g. Fig. 2B vs 2A.

3.3. Status epilepticus induces gliosis in the affected area

Immunoreactivity for astrocytic marker glial fibrillary acidic protein (GFAP) was increased in the post-FSE cortex at the site of convulsant application vs saline control at 10 and 30d post FSE (Fig. 3, Tables1 and 2). Significant microgliosis was also present at both time points after FSE (Fig.S1). The glial reaction included an increase in hypertrophic astrocytes that had elongated cell bodies and thicker processes (red in Fig. 3B, B1; E, E1). As shown in Fig. 3G, the percentage pixel area of GFAP-IR was increased 10 and 30d after the induction of FSE (Tables 1 and 2). Activation of astrocytes can release astrocyte-secreted proteins such as thrombospondins (TSPs) that are one factor involved in the development of new excitatory synapses (Christopherson et al., 2005; Eroglu et al., 2009). TSP2-IR was increased 10 and 30d after FSE induction (Tables 1 and 2) (Fig. 3A vs; B, B1; D vs, E, E1; H). There was also an increase in TSP receptor α2δ-1 in the gliotic cortex 10d and 30d post-FSE (Tables 1 and 2) (Fig. 4 A, Ai; B, Bi; C, D).

3.4. Effects of FSE on excitatory synaptic connectivity

To test whether the increases in TSP2 and α2δ-1 were associated with an increase in excitatory synapses, we measured close appositions of presynaptic and postsynaptic markers, VGLUT1- and PSD95-IR (putative excitatory synapses (Eroglu et al., 2009)) in cortical layer V of control and 10d and 30d post FSE sections (Fig. 5). Both VGLUT1- and PSD95-IR were increased 10d post FSE (cf Fig. 5A-A1 and 5B-Bi) (VGLUT1 control 7% ± 2%, n = 13 sections from 3 animals; FSE 18.7% ± 2%, n = 14 sections from 4 animals; p = .004 Mann-Whitney test; PSD95 control 9.1% ± 2%, n = 13 sections from 3 animals; FSE 17.4% ± 2%, n = 14 sections from 4 animals; p = .042 Mann-Whitney test). The percentage of the colocalization area between VGLUT1- and PSD95-IR per ROI at 10 and 30 d post-FSE (yellow puncta; examples in white circles in Fig. 5A-B, Ai-Bi and Aii-Bii) was increased at both time points post-FSE (Tables 1 and 2) (Fig. 5Ai, Bi). The results support the conclusion that there is an increase in density of excitatory synapses in neocortex lasting at least 30d following prolonged FSE.

To determine whether the increases in VGLUT1- PSD95 colocalizations induced by a single episode of FSE were associated with increases in functional glutamatergic synaptic excitation, we recorded spontaneous (s)EPSCs and miniature (m)EPSCs from layer V_A pyramidal (Pyr) neurons 10 and 30d after the induction of FSE and from age matched controls (Fig. 6). Ten and 30d post-FSE, the frequency but not the amplitude of spontaneous (s)EPSCs increased compared to controls (excluding burst discharges) (Tables 3 and 4) (Fig. 6 A, B; D, E; G, H). The increase in sEPSC frequency was not associated with a significant change in input resistance (Rm: 214.8 ± 47MΩ, n = 8 in control from 4 animals; 208.7 ± 18MΩ n = 15 in FSE + saline 30d post-SE in 5 animals, ns). mEPSC frequency in 1 μM TTX in FSE animals was increased at both time points without a change in amplitude (Fig. 6 I, J; L, M; O, P) (Tables 3 and 4). These results indicate that there are increases in action-potential evoked excitatory synaptic transmission after the FSE induction, as well as changes in mEPSC frequency, due, at least in part, to increased numbers of synaptic contacts (Fig. 5).

3.5. Decreased frequency of mIPSCs after FSE

Another consequence of prolonged seizures in SE might be decreases in function or loss of inhibitory interneurons as occurs in hippocampal models of temporal lobe epilepsy (e.g.; (Kobayashi and Buckmaster, 2003; Sloviter, 1987; Zhang and Buckmaster, 2009)). Counts of PV interneurons were made in ROIs extending from the pial surface (Fig. 7A-D, white dashed lines) to the junction between layer VI and the white matter. Fig. 7E-F shows that the number of PV-IR neurons/μm^2 in the affected area is decreased at 10 and 30d post-FSE (Fig. 7E: 10 d: control 33 ± 2 neurons, n = 15 sections from 4 animals; FSE 20 ± 1, n = 12 sections from 4 animals; p < .0001; F: *30 d*: control 36 ± 2, n = 10 sections from 4 animals; FSE 18 ± 2, n = 8 sections from 4 animals; p < .001). To determine whether these anatomical abnormalities were associated with decreases in functional inhibition, we measured the frequency and amplitude of mIPSCs in layer V_A pyramidal neurons in slices from cortex of 10d post-FSE (Methods). Results (Fig. 7G, H) showed that the frequency but not the amplitude of mIPSCs was decreased 10d post FSE (control 13.03 ± 1.79 Hz n = 16 from 5 animals; FSE 6.02 ± 0.68 Hz n = 14 from 5 animals; unpaired t-test, p = .002). In summary, ICC and electrophysiological data indicate that there is a long lasting increase in

excitatory and decrease in inhibitory connectivity and function in the area of pharmacologically-induced FSE.

3.6. Focal SE increases the incidence of evoked epileptiform field potentials

Maladaptive synaptic rearrangements can lead to the formation of aberrant network excitability. To determine whether this occurred after FSE in this model, we obtained local field potential recordings from in vitro slices in control and 10 and 30d post-FSE. Extracellular bipolar 0.1 Hz single 100 μs current pulses were delivered at increasing intensities (up to 3 × threshold; 0.75–3 μA) to the white matter/layer VI junction and responses recorded on column from layer V. Epileptiform field potentials, consisting of long, variable latency, all-or-none polyphasic bursts of field potentials with durations of ≥100 milliseconds, were evoked at or near threshold stimulation and he threshold stimulus intensity required to evoke epileptiform discharges was often lower than that necessary to evoke a minimal field response in control animals (Fig. 8B, F). The amplitude of evoked bursts increased with stimulus intensity, up to 3 × threshold. Prolonged spontaneous burst discharges associated with unit activity occurred infrequently (Fig. 8D). These events resembled the “epileptiform” responses in partially isolated cortex (Graber and Prince, 2004; Prince and Tseng, 1993; Sen et al., 2018), and were not recorded in slices from control animals. We used the “coastline index” of the LFP (Methods, (Korn et al., 1987) as a measure of circuit activity in control and 10 and 30d post FSE. This index increased at 10d and 30d post-FSE (10d: control 2.8 ± 0.3, n = 14 slices from 4 animals; FSE epileptiform responses: 37.9 ± 16, $n = 7$ slices from 6 animals; $p = .012$; 30d: control 4.8 ± 0.3, $n = 20$ slices from 6 animals; FSE epileptiform 22.57 ± 6, $n = 15$ sections from 7 animals $p = .0001$) (Fig. 8 I, J). Analysis of the percentage of mice in which epileptiform bursts could be evoked, or the percentage of burst-generating slices/mouse, suggested that hyperexcitability persisted for at least 30d post-SE (Fig. 8H). Epileptiform burst discharges were recorded in slices from 2 mice 100d post FSE (Fig. 8G), supporting the conclusion that the aberrant increases in cortical network excitability were chronically present post-SE. These results are consistent with the increases in excitatory synaptic connectivity shown in Figs. 5 and 6 and the reduction in mIPSCs (Fig. 7).

3.7. Gabapentin treatment prevents FSE-induced increases in excitatory connectivity

Gabapentin decreases excitatory synaptogenesis during early development (Eroglu et al., 2009) and can also decrease excitatory synaptic activity and epileptogenesis in injury-induced rodent focal neocortical epilepsy models (Andresen et al., 2014; Li et al., 2012; Takahashi et al., 2018). GBP treatment following FSE also decreases structural alterations and seizure severity in the limbic system following pilocarpine induced SE (Rossi et al., 2017; Rossi et al., 2013). To determine whether GBP would have similar effects in the FSE model, we treated mice with GBP (ip 100 mg/kg/day 3×/day for 7d) beginning 3 h after the onset of FSE. This dose is in the range that has been used ip in rats (Gillin and Sorkin, 1998; Li et al., 2012) and did not result in significant decrease in spontaneous activity. GBP-treated mice were allowed to recover for 10 or 30d after the induction of FSE and then processed for ICC experiments. Results showed that the 7d GBP treatment was associated with a significant reduction of GFAP-IR, measured 10 d post-FSE (Tables 1 & 2; Fig. 3 Ai vs Aii), that persisted for at least 30d (Fig. 3Bi vs Bii; C, D). In addition, there was a significant

decrease of α2δ-1 at both time points (Tables 1 & 2; Fig. 4 Aii, Bii vs Ai,Bi, C, D). GBP treatment prevented the FSE-induced increase of close appositions between VGLUT1 and PSD95 puncta at both time points (Fig. 5 Ai vs Aii, Bi vs Bii; C, D). These structural changes were associated with reduced frequency of sEPSCs and mEPSCs 10 and 30d post-FSE (Tables 3 and 4; Fig. 6 A-H, I-P). Results show that GBP treatment, begun after FSE, has prolonged effects to suppress astrogliosis and decrease structural and functional increases in excitatory synaptogenesis induced by the prolonged seizure activity.

4. Discussion

Status epilepticus results in complex pathophysiological alterations in brain, including cell loss (Hofmann, 2016), alterations in the blood brain barrier (Friedman et al., 2009; Gorter et al., 2015; Han et al., 2017; Rossi et al., 2017), activation of astrocytes and microglia (Rossi et al., 2013; Vargas-Sanchez et al., 2018; Walker, 2018), and inflammatory and immune cascades (De Simoni et al., 2000; Iori et al., 2016; Rossi et al., 2017; Vezzani et al., 2016). Such abnormalities presumably result in long term sequelae in survivors, including disordered cognition, development of epilepsy de novo or worsening of existing seizures. Therapy of the acute SE episode is directed toward stopping seizures, while prophylaxis of long-term consequences has received less attention. Most experiments focused on abnormalities post-SE have used models of generalized seizures and assessed effects in the hippocampal-limbic system. Acute neuropathological alterations have been reported in sensorimotor cortex and thalamus of rats killed after 2 h of focal seizures in a similar model (Collins and Olney, 1982); however, less is known about longer-term anatomical or electrophysiological effects of neocortical FSE. To investigate this issue, we used ICC and electrophysiological techniques to assess delayed pathophysiological consequences in a model of neocortical FSE. Neuronal injury was present 10 d post-FSE, evidenced by 1) a reduction in the total number of neurons immuno-labeled with NeuN; 2) decreased density of PV-IR positive interneurons and the frequency of mIPSCs; 3) astrogliosis and microgliosis; 4) increases in expression of synaptogenic proteins TSP2- and α2δ-1-IR; 5) increases in functional excitatory connectivity and 6) hyperexcitability in neocortical networks in vitro. We did not assess the time of onset of these neocortical abnormalities; however, it is likely that some are present early post-FSE (Collins and Olney, 1982; Meldrum and Brierley, 1972). These changes persisted for at least 30d post-FSE and were significantly reduced by 7 days of GBP treatment beginning on the day of FSE.

4.1. Neuronal injury after neocortical status epilepticus

As reported in other epilepsy models and in human temporal lobe epilepsy, SE can induce cell loss or alterations in function and structure of surviving neurons (Buckmaster et al., 2017; Cavazos et al., 1994; Du et al., 1995; Du et al., 1993; Zhang and Buckmaster, 2009). Our results document loss of ~53% of all neurons in the affected area (Fig. 2) and ~ 37% of PV inhibitory neurons 10d post-FSE (Fig. 7). Reductions in PV neurons 30d post-FSE were not significantly different from those at 10d, suggesting that inhibitory cell loss was not progressive, at least over several weeks. Both cell death and decreases in PV immunoreactivity may have contributed to decreased density of PV-IR neurons (e.g. (Kawaguchi and Kondo, 2002; Rosen et al., 1998) and associated reduction in mIPSC

frequency (Fig. 7). It is possible that sprouting of inhibitory axons and compensatory increases in inhibitory function occur at later times following FSE-induced injury, as in other epilepsy models (Bausch, 2005; Peng et al., 2013) and human epilepsy (Bausch, 2005; Magloczky, 2010). The loss of the excitatory neurons is offset by an increase in excitatory synaptogenesis (Fig. 6) that is, in turn, associated with generation of epileptiform bursts in slices. Sprouting of excitatory axons, as in other models of cortical injury and epilepsy (e.g. (Kusmierczak et al., 2015; Salin et al., 1995; Tauck and Nadler, 1985), and/or increases in neurotransmitter release at excitatory terminals (Faria et al., 2017), are potential explanations for the apparent difference in effects of FSE on excitatory cell counts vs excitatory synaptic activity. Immunoreactivity for heavy chain neurofilaments was markedly increased in post-SE cortex (not shown), as an indication of axonal injury and sprouting (Christman et al., 1997).

4.2. Focal SE leads to astrogliosis and release of astrocytic synaptogenic proteins

Blood brain barrier breakdown (Ivens et al., 2007; Ralay Ranaivo and Wainwright, 2010; Tomkins et al., 2007), such as occurs in SE, can result in entry of serum albumin that in turn activates astrocytes and other processes that induce epileptogenesis (reviewed in (Friedman et al., 2009). In this, as in other epilepsy animal models (Andresen et al., 2014; Li et al., 2012; Rossi et al., 2017; Rossi et al., 2013; Seiffert et al., 2004), astrogliosis is prominent and likely contributes to increased excitatory synapse formation, aberrant connectivity and hyperexcitability through release of synaptogenic proteins (Christopherson et al., 2005; Eroglu et al., 2009; Farhy-Tselnicker et al., 2017; Li et al., 2012; Risher and Eroglu, 2012), such as TSPs that bind to their α2δ1 receptors (Fig. 3). Our results show that FSE leads to increases in both TSP2 and α2δ-1, likely resulting in the increased number of putative excitatory synapses (Risher and Eroglu, 2012; Risher et al., 2018). Overexpression of the α2δ-1 protein in the partial cortical isolation model and in transgenic mice is associated with epileptiform activity and increased excitatory connectivity in in vitro slices, as well as spontaneous EEG epileptiform activity and non-convulsive seizures in vivo (Faria and Prince, 2010; Li et al., 2012). Other astrocyte-secreted proteins such as hevin (Kucukdereli et al., 2011) and glypicans 4 and 6 (Farhy-Tselnicker et al., 2017) may contribute to excitatory synaptogenesis in neocortical FSE and other models of cortical injury.

4.3. Status epilepticus promotes hyperexcitability in cortical networks

In the present study, the long-lasting increases in colocalized VGLUT1-IR and PSD95-IR puncta, together with increased frequency of sEPSCs and mEPSCs and occurrence of epileptiform burst activity, indicate the development of aberrant excitatory synaptic connectivity within cortical networks. Decreased density of PV interneurons and the frequency of mIPSCs, suggests that disinhibition contributes to the hyperexcitability, as in other models (Gu et al., 2017; Jin et al., 2014; Sen et al., 2018) and in human epileptogenic lesions (de Lanerolle et al., 1989; DeFelipe, 1999; Marco et al., 1996; Medici et al., 2016). The increase in excitatory connectivity following neocortical FSE in these experiments is common in other epilepsy models (Dancause et al., 2005; Marco and DeFelipe, 1997; Shao and Dudek, 2004; Takahashi et al., 2016; Tauck and Nadler, 1985) and human epileptic tissue (Marco and DeFelipe, 1997). Cortical injury and loss of excitatory neurons is

accompanied by axonal sprouting, new excitatory connectivity, functional circuit restructuring and abnormal network activity.

4.4. Comparable consequences of clinical and experimental FSE

Similarities between effects of FSE in this model and human FSE include injury to interneurons and pyramidal cells), necrosis and gliosis in the SE focus and in its interconnected brain areas, and development of hyperexcitability in some cases. Following FSE, patients may develop brain lesions that can result in focal chronic epilepsy (Bartolomei et al., 1999). It is often unclear whether the damage observed in the human brain post-SE is due to a preexisting condition. However, Fujikawa et al. reported 3 clinical cases of FSE in the absence of systemic complications or preexisting epilepsy in which there was widespread gliosis and neuronal loss in hippocampus and other limbic structures, neocortex, cerebellum and thalamus (Fujikawa et al., 2000). Some of the consequences of FSE in humans are similar to those observed in this FSE mouse model. It is important to have realistic animal models in which to study the consequences of a single episode of SE and explore potential treatments to prevent injury, pileptogenesis and other long-term sequelae.

4.5. Gabapentin treatment prevents morphological abnormalities post-FSE

In addition to known actions to decrease excitatory synapse formation during development (Eroglu et al., 2009), gGABApentin has multiple other effects in models of cortical and hippocampal injury (Li et al., 2012); (Lau et al., 2017); (Rossi et al., 2017). In this FSE model, GBP treatment resulted in a decrease of presumptive excitatory synapses (colocalized VGLUT-PSD95-IR), as well as GFAP-, TSP2- and α2δ-1-IR, assessed 10d post-FSE. This reduction can be related in part to anti-synaptogenic effects of GBP through binding to the α2δ-1 TSP receptor. Some effects of the GBP treatment were present at least 30d post-FSE (Figs. 3-6). Mechanisms underlying these long-lasting effects of relatively brief treatment are unclear. During development, GBP interferes with newly-formed but not well-established synapses (Eroglu et al., 2009). This might suggest that some of the epileptogenic processes induced by FSE or other GBP-responsive cortical injuries (e.g. (Andresen et al., 2014; Li et al., 2012; Rossi et al., 2013) are temporally restricted. It will be important to determine whether anti-synaptogenic effects of GBP are limited to a critical period post-injury.

4.6. Astrogliosis and GBP effects

Brain injury activates microglia that release chemokines and cytokines, known to induce gliosis. Gabapentin treatment may suppress glial activation through several mechanisms, including decreased release of fractalkine CX3CL1 (Yang et al., 2012), effects to reduce cell death (Li et al., 2012), decreasing the alterations in blood-brain barrier (Rossi et al., 2017). Gabapentin may also impair anterograde trafficking of α2δ1 and reduce its cell surface expression (Bauer et al., 2009).

Long-term functional consequences of prolonged seizure activity occur in this and in other epilepsy models of SE, as well as in clinical SE (references above). Of interest will be results of studies on potential behavioral changes in the post-FSE model and effects of GBP as prophylactic treatment for alterations in behavior. It will also be important to obtain

chronic recordings from implanted mice to determine whether the hyperactivity we found in in vitro slices post-FSE is progressive and associated with behavioral seizures in vivo, as occur following SE in man.

Gabapentinoids are protective against injury and antiepileptogenic in a number of models (Andresen et al., 2014; Lau et al., 2017; Rossi et al., 2013), (reviewed in Klein, 2020) raising the question of their potential use as prophylactic agents in man, e.g. following brain trauma, other disease processes, or SE. Should gabapentinoids be used as prophylactic agents in patients following an episode of status epilepticus? One fundamental issue regarding such use is the potential role of new excitatory connectivity after injury as an adaptive response that promotes recovery of function (e.g. Buchli and Schwab, 2005; Dancause et al., 2005; Darian-Smith and Gilbert, 1994), vs a maladaptive one promoting epileptogenesis. Also, more needs to be known about anatomical and functional consequences of FSE in structures remote from the primary site of seizure activity, where new excitatory connectivity might activate circuits that can suppress cortical excitability (Motelow et al., 2015).

5. Conclusions

In neocortical focal SE, seizures per se, without a prior cortical lesion, induce long-lasting structural and functional abnormalities and epileptogenic activity through a variety of pathophysiological mechanisms. Experimental results show that GBP treatment for 7d following a prolonged episode of FSE, has long-term actions that limit maladaptive seizure-induced excitatory synaptogenesis and other effects of SE. This and other reported neuroprotective actions suggest that GBP may be a promising prophylactic drug to limit consequences of severe and prolonged seizures.

Supplementary Material

Refer to Web version on PubMed Central for supplementary material.

Acknowledgments

We thank Isabel Parada for performing and analyzing the ICC experiments and Reza Moein Taghavi for software development. Whitney McDonald and Karina Scolise performed pilot experiments in the FSE model. This work was supported by a fellowship from the American Epilepsy Society (M-B P-R); NINDS grant NS090076 from the National Institutes of Health (DAP) and the Edward and Irene Pimley Research Fund.

Abbreviations:

EEG	electroencephalogram
FSE	focal status epilepticus
GBP	gabapentin
ICC	immunocytochemistry
IR	immunoreactivity
PSD95	postsynaptic density protein 95

SE	status epilepticus
Vglutl	vesicular glutamate transporter 1

References

Andresen L, et al., 2014. Gabapentin attenuates hyperexcitability in the freeze-lesion model of developmental cortical malformation. Neurobiol. Dis 71, 305–316. [PubMed: 25158291]

Ayala GF, et al., 1970. Excitability changes and inhibitory mechanisms in neocortical neurons during seizures. J. Neurophysiol 33, 73–85. [PubMed: 4312440]

Baracskay P, et al., 2008. Generalization of seizures parallels the formation of “dark” neurons in the hippocampus and pontine reticular formation after focal-cortical application of 4-aminopyridine (4-AP) in the rat. Brain Res. 1228, 217–228. [PubMed: 18602900]

Bartolomei F, et al., 1999. Development of focal chronic epilepsy following focal status epilepticus in adult patients. Neurophysiol. Clin 29, 271–276. [PubMed: 10431292]

Bauer CS, et al., 2009. The increased trafficking of the calcium channel subunit alpha2delta-1 to presynaptic terminals in neuropathic pain is inhibited by the alpha2delta ligand pregabalin. J. Neurosci 29, 4076–4088. [PubMed: 19339603]

Bausch SB, 2005. Axonal sprouting of GABAergic interneurons in temporal lobe epilepsy. Epilepsy Behav. 7, 390–400. [PubMed: 16198153]

Buchli AD, Schwab ME, 2005. Inhibition of Nogo: a key strategy to increase regeneration, plasticity and functional recovery of the lesioned central nervous system. Ann. Med 37, 556–567. [PubMed: 16338758]

Buckmaster PS, et al., 2017. Seizure frequency correlates with loss of dentate gyrus GABAergic neurons in a mouse model of temporal lobe epilepsy. J. Comp. Neurol 525, 2592–2610. [PubMed: 28425097]

Cavazos J, et al., 1994. Neuronal loss induced in limbic pathways by kindling: evidence for induction of hippocampal sclerosis by repeated brief seizures. J. Neurosci 14, 3106–3121. [PubMed: 8182460]

Christman CW, et al., 1997. Characterization of a prolonged regenerative attempt by diffusely injured axons following traumatic brain injury in adult cat: a light and electron microscopic immunocytochemical study. Acta Neuropathol. (Berl.) 94, 329–337. [PubMed: 9341933]

Christopherson KS, et al., 2005. Thrombospondins are astrocyte-secreted proteins that promote CNS synaptogenesis. Cell 120, 421–433. [PubMed: 15707899]

Collins RC, Olney JW, 1982. Focal cortical seizures cause distant thalamic lesions. Science 218, 177–179. [PubMed: 7123229]

Dancause N, et al., 2005. Extensive cortical rewiring after brain injury. J. Neurosci 25, 10167–10179. [PubMed: 16267224]

Darian-Smith C, Gilbert CD, 1994. Axonal sprouting accompanies functional reorganization in adult cat striate cortex. Nature 368, 737–740. [PubMed: 8152484]

de Lanerolle NC, et al., 1989. Hippocampal interneuron loss and plasticity in human temporal lobe epilepsy. Brain Res. 495, 387–395. [PubMed: 2569920]

De Simoni MG, et al., 2000. Inflammatory cytokines and related genes are induced in the rat hippocampus by limbic status epilepticus. Eur. J. Neurosci 12, 2623–2633. [PubMed: 10947836]

DeFelipe J, 1999. Chandelier cells and epilepsy. Brain 122 (Pt 10), 1807–1822. [PubMed: 10506085]

DeLorenzo RJ, et al., 1995. Epidemiology of status epilepticus. J. Clin. Neurophysiol 12, 316–325. [PubMed: 7560020]

Du F, et al., 1993. Preferential neuronal loss in layer III of the entorhinal cortex in patients with temporal lobe epilepsy. Epilepsy Res. 16, 223–233. [PubMed: 8119273]

Du F, et al., 1995. Preferential neuronal loss in layer III of the medial entorhinal cortex in rat models of temporal lobe epilepsy. J. Neurosci 15, 6301–6313. [PubMed: 7472396]

Eroglu C, et al., 2009. Gabapentin receptor alpha2delta-1 is a neuronal thrombospondin receptor responsible for excitatory CNS synaptogenesis. Cell 139, 380–392. [PubMed: 19818485]

Farhy-Tselnicker I, et al., 2017. Astrocyte-secreted Glypican 4 regulates release of neuronal Pentraxin 1 from axons to induce functional synapse formation. Neuron 96 (428–445), e13. [PubMed: 29024665]

Faria LC, Prince DA, 2010. Presynaptic inhibitory terminals are functionally abnormal in a rat model of posttraumatic epilepsy. J. Neurophysiol 104, 280–290. [PubMed: 20484536]

Faria LC, et al., 2017. Epileptiform activity and behavioral arrests in mice overexpressing the calcium channel subunit alpha2delta-1. Neurobiol. Dis 102, 70–80. [PubMed: 28193459]

Feng B, Chen Z, 2016. Generation of febrile seizures and subsequent Epileptogenesis. Neurosci. Bull 32, 481–492. [PubMed: 27562688]

Franklin KBJ, Paxinos G, 1997. The Mouse Brain in Stereotaxic Coordinates. Academic Press, San Diego.

Friedman A, et al., 2009. Blood-brain barrier breakdown-inducing astrocytic transformation: novel targets for the prevention of epilepsy. Epilepsy Res. 85, 142–149. [PubMed: 19362806]

Fujikawa DG, et al., 2000. Status epilepticus-induced neuronal loss in humans without systemic complications or epilepsy. Epilepsia 41, 981–991. [PubMed: 10961625]

Gillin S, Sorkin LS, 1998. Gabapentin reverses the allodynia produced by the administration of anti-GD2 ganglioside, an immunotherapeutic drug. Anesth. Analg 86, 111–116. [PubMed: 9428862]

Gorter JA, et al., 2015. Status epilepticus, blood-brain barrier disruption, inflammation, and epileptogenesis. Epilepsy Behav. 49, 13–16. [PubMed: 25958228]

Graber KD, Prince DA, 2004. A critical period for prevention of posttraumatic neocortical hyperexcitability in rats. Ann. Neurol 55, 860–870. [PubMed: 15174021]

Gu F, et al., 2017. Structural alterations in fast-spiking GABAergic interneurons in a model of posttraumatic neocortical epileptogenesis. Neurobiol. Dis 108, 100–114. [PubMed: 28823934]

Han H, et al., 2017. Breaking bad: the structure and function of the blood-brain barrier in epilepsy. AAPS J. 19, 973–988. [PubMed: 28550637]

Hesdorffer DC, et al., 1998. Risk of unprovoked seizure after acute symptomatic seizure: effect of status epilepticus. Ann. Neurol 44, 908–912. [PubMed: 9851435]

Hofmann G, et al., 2016. Hilar somatostatin interneuron loss reduces dentate gyrus inhibition in a mouse model of temporal lobe epilepsy. Epilepsia 57 (6), 977–983. [PubMed: 27030321]

Holtkamp M, et al., 2005. Predictors and prognosis of refractory status epilepticus treated in a neurological intensive care unit. J. Neurol. Neurosurg. Psychiatry 76, 534–539. [PubMed: 15774441]

Iori V, et al., 2016. Modulation of neuronal excitability by immune mediators in epilepsy. Curr. Opin. Pharmacol 26, 118–123. [PubMed: 26629681]

Ivens S, et al., 2007. TGF-beta receptor-mediated albumin uptake into astrocytes is involved in neocortical epileptogenesis. Brain 130, 535–547. [PubMed: 17121744]

Jin X, et al., 2014. Excitatory and inhibitory synaptic connectivity to layer V fast-spiking interneurons in the freeze lesion model of cortical microgyria. J. Neurophysiol 112, 1703–1713. [PubMed: 24990567]

Kawaguchi Y, Kondo S, 2002. Parvalbumin, somatostatin and cholecystokinin as chemical markers for specific GABAergic interneuron types in the rat frontal cortex. J. Neurocytol 31, 277–287. [PubMed: 12815247]

Klein P, et al., 2020. Repurposed molecules for antiepileptogenesis: Missing an opportunity to prevent epilepsy? Epilepsia 61 (3), 359–386. [PubMed: 32196665]

Kobayashi M, Buckmaster PS, 2003. Reduced inhibition of dentate granule cells in a model of temporal lobe epilepsy. J. Neurosci 23, 2440–2452. [PubMed: 12657704]

Korn SJ, et al., 1987. Epileptiform burst activity induced by potassium in the hippocampus and its regulation by GABA-mediated inhibition. J. Neurophysiol 57, 325–340. [PubMed: 3559679]

Kucukdereli H, et al., 2011. Control of excitatory CNS synaptogenesis by astrocyte-secreted proteins Hevin and SPARC. Proc. Natl. Acad. Sci 108, E440–E449. [PubMed: 21788491]

Kusmierczak M, et al., 2015. Changes in long-range connectivity and neuronal reorganization in partial cortical deafferentation model of epileptogenesis. Neuroscience 284, 153–164. [PubMed: 25304932]

Lau LA, et al., 2017. alpha2delta-1 signaling drives cell death, synaptogenesis, circuit reorganization, and gabapentin-mediated neuroprotection in a model of insult-induced cortical malformation. eNeuro 4.

Li H, et al., 2012. Gabapentin decreases epileptiform discharges in a chronic model of neocortical trauma. Neurobiol. Dis 48, 429–438. [PubMed: 22766033]

Magloczky Z, 2010. Sprouting in human temporal lobe epilepsy: excitatory pathways and axons of interneurons. Epilepsy Res. 89, 52–59. [PubMed: 20149961]

Marco P, DeFelipe J, 1997. Altered synaptic circuitry in the human temporal neocortex removed from epileptic patients. Exp. Brain Res 114, 1–10. [PubMed: 9125446]

Marco P, et al., 1996. Inhibitory neurons in the human epileptogenic temporal neocortex. An immunocytochemical study. Brain 119 (Pt 4), 1327–1347. [PubMed: 8813295]

Medici V, et al., 2016. Different parvalbumin and GABA expression in human epileptogenic focal cortical dysplasia. Epilepsia 57, 1109–1119. [PubMed: 27173597]

Meldrum BS, Brierley JB, 1972. Neuronal loss and gliosis in the hippocampus following repetitive epileptic seizures induced in adolescent baboons by allylglycine. Brain Res. 48, 361–365. [PubMed: 4630226]

Motelow JE, et al., 2015. Decreased subcortical cholinergic arousal in focal seizures. Neuron 85, 561–572. [PubMed: 25654258]

Patterson KP, et al., 2014. Origins of temporal lobe epilepsy: febrile seizures and febrile status epilepticus. Neurotherapeutics 11, 242–250. [PubMed: 24604424]

Peng Z, et al., 2013. A reorganized GABAergic circuit in a model of epilepsy: evidence from optogenetic labeling and stimulation of somatostatin interneurons. J. Neurosci 33, 14392–14405. [PubMed: 24005292]

Prince DA, Tseng GF, 1993. Epileptogenesis in chronically injured cortex: in vitro studies. J. Neurophysiol 69, 1276–1291. [PubMed: 8492163]

Ralay Ranaivo H, Wainwright MS, 2010. Albumin activates astrocytes and microglia through mitogen-activated protein kinase pathways. Brain Res. 1313, 222–231. [PubMed: 19961838]

Risher WC, Eroglu C, 2012. Thrombospondins as key regulators of synaptogenesis in the central nervous system. Matrix Biol. 31, 170–177. [PubMed: 22285841]

Risher WC, et al., 2018. Thrombospondin receptor alpha2delta-1 promotes synaptogenesis and spinogenesis via postsynaptic Rac1. J. Cell Biol 217, 3747–3765. [PubMed: 30054448]

Rosen GD, et al., 1998. Effects of neonatal freeze lesions on expression of parvalbumin in rat neocortex. Cereb. Cortex 8, 753–761. [PubMed: 9863702]

Rossi AR, et al., 2013. Gabapentin administration reduces reactive gliosis and neurodegeneration after pilocarpine-induced status epilepticus. PLoS One 8, e78516. [PubMed: 24250797]

Rossi A, et al., 2017. Early gabapentin treatment during the latency period increases convulsive threshold, reduces microglial activation and macrophage infiltration in the lithium-pilocarpine model of epilepsy. Pharmaceuticals 10, 93.

Salin P, et al., 1995. Axonal sprouting in layer V pyramidal neurons of chronically injured cerebral cortex. J. Neurosci 15, 8234–8245. [PubMed: 8613757]

Santamarina E, et al., 2015. Prognosis of status epilepticus (SE): relationship between SE duration and subsequent development of epilepsy. Epilepsy Behav. 49, 138–140. [PubMed: 26117525]

Seiffert E, et al., 2004. Lasting blood-brain barrier disruption induces epileptic focus in the rat somatosensory cortex. J. Neurosci 24, 7829–7836. [PubMed: 15356194]

Sen O, et al., 2018. Mid-term results of peripheral cannulation after robotic cardiac surgery. Braz. J. Cardiovasc. Surg 33, 443–447. [PubMed: 30517251]

Shao L-R, Dudek FE, 2004. Increased excitatory synaptic activity and local connectivity of hippocampal CA1 pyramidal cells in rats with Kainate-induced epilepsy. J. Neurophysiol 92, 1366–1373. [PubMed: 15084640]

Silva AV, et al., 2005. Neocortical and hippocampal changes after multiple pilocarpine-induced status epilepticus in rats. Epilepsia 46, 636–642. [PubMed: 15857427]

Sloviter RS, 1987. Decreased hippocampal inhibition and a selective loss of interneurons in experimental epilepsy. Science 235, 73–76. [PubMed: 2879352]

Takahashi DK, et al., 2016. Aberrant excitatory rewiring of layer V pyramidal neurons early after neocortical trauma. Neurobiol. Dis 91, 166–181. [PubMed: 26956396]

Takahashi DK, et al., 2018. Gabapentin prevents progressive increases in excitatory connectivity and Epileptogenesis following neocortical trauma. Cereb. Cortex 28, 2725–2740. [PubMed: 28981586]

Tauck D, Nadler J, 1985. Evidence of functional mossy fiber sprouting in hippocampal formation of kainic acid-treated rats. J. Neurosci 5, 1016–1022. [PubMed: 3981241]

Teskey GC, et al., 1999. Sex differences in cortical plasticity and behavior following anterior cortical kindling in rats. Cereb. Cortex 9, 675–682. [PubMed: 10554990]

Tomkins O, et al., 2007. Blood-brain barrier disruption results in delayed functional and structural alterations in the rat neocortex. Neurobiol. Dis 25, 367–377. [PubMed: 17188501]

Vargas-Sanchez K, et al., 2018. Astroglial role in the pathophysiology of status epilepticus: an overview. Oncotarget 9, 26954–26976. [PubMed: 29928494]

Vezzani A, et al., 2016. Infections, inflammation and epilepsy. Acta Neuropathol. 131, 211–234. [PubMed: 26423537]

Walker MC, 2018. Pathophysiology of status epilepticus. Neurosci. Lett 667, 84–91. [PubMed: 28011391]

Yang X-F, Rothman SM, 2001. Focal cooling rapidly terminates experimental neocortical seizures. Ann. Neurol 49, 721–726. [PubMed: 11409423]

Yang JL, et al., 2012. Gabapentin reduces CX3CL1 signaling and blocks spinal microglial activation in monoarthritic rats. Mol. Brain 5, 18. [PubMed: 22647647]

Zhang W, Buckmaster PS, 2009. Dysfunction of the dentate basket cell circuit in a rat model of temporal lobe epilepsy. J. Neurosci 29, 7846–7856. [PubMed: 19535596]

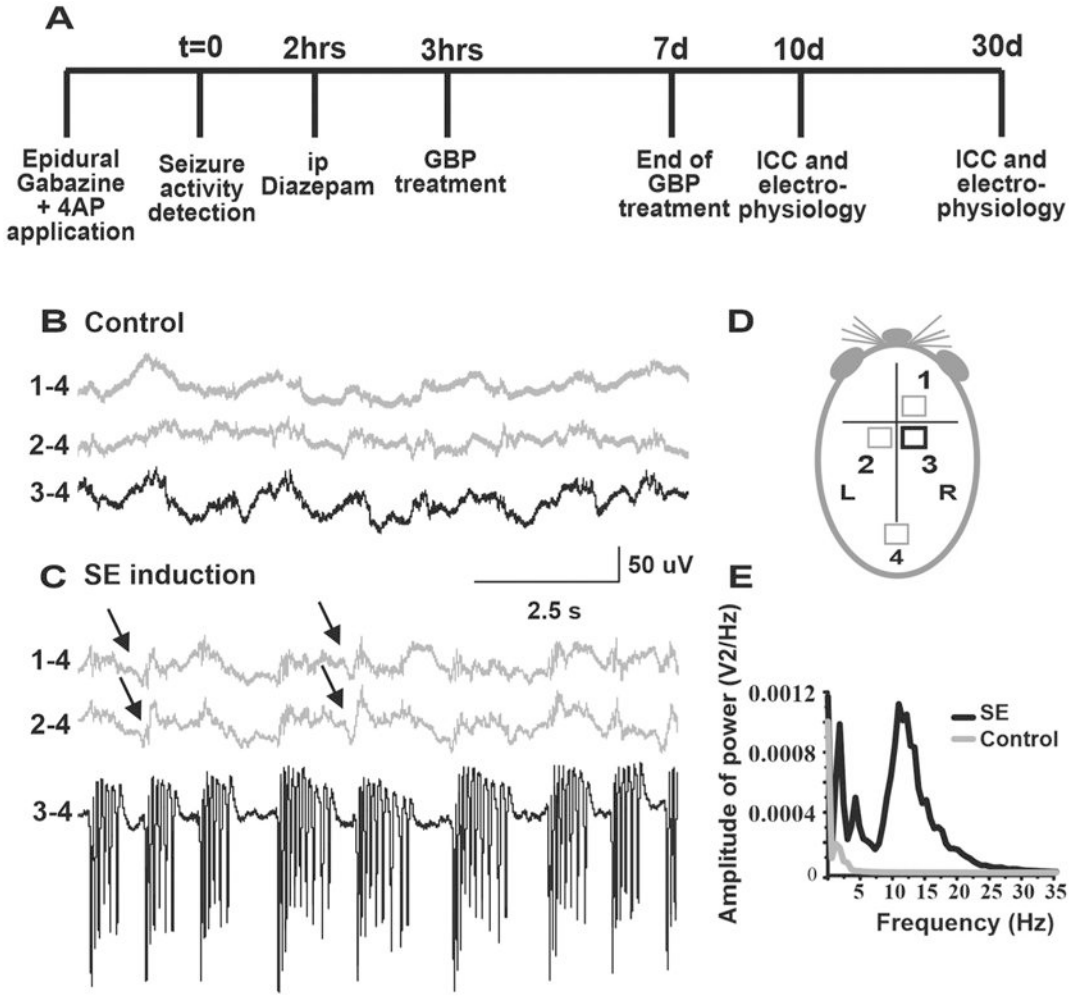

Fig. 1.

FSE induced by focal convulsant drug application to somatosensory cortex. A: Experimental timeline. B-C: EEG recordings from an anesthetized mouse before (B) and during focal status epilepticus (C). Electrode placement shown in D. Indifferent electrode 4 over cerebellum. Electrode 3 at site of gabazine/4AP epidural application (black box). Bursts of epileptiform spike activity in C, lead 3–4, were accompanied by contralateral focal myoclonic activity. C1–4 and 2–4: Low amplitude projected spikes (arrows) anterior and contralateral to the focus. E: EEG power analysis during focal continuous spike activity (black); compared to brain activity prior to drug application (gray).

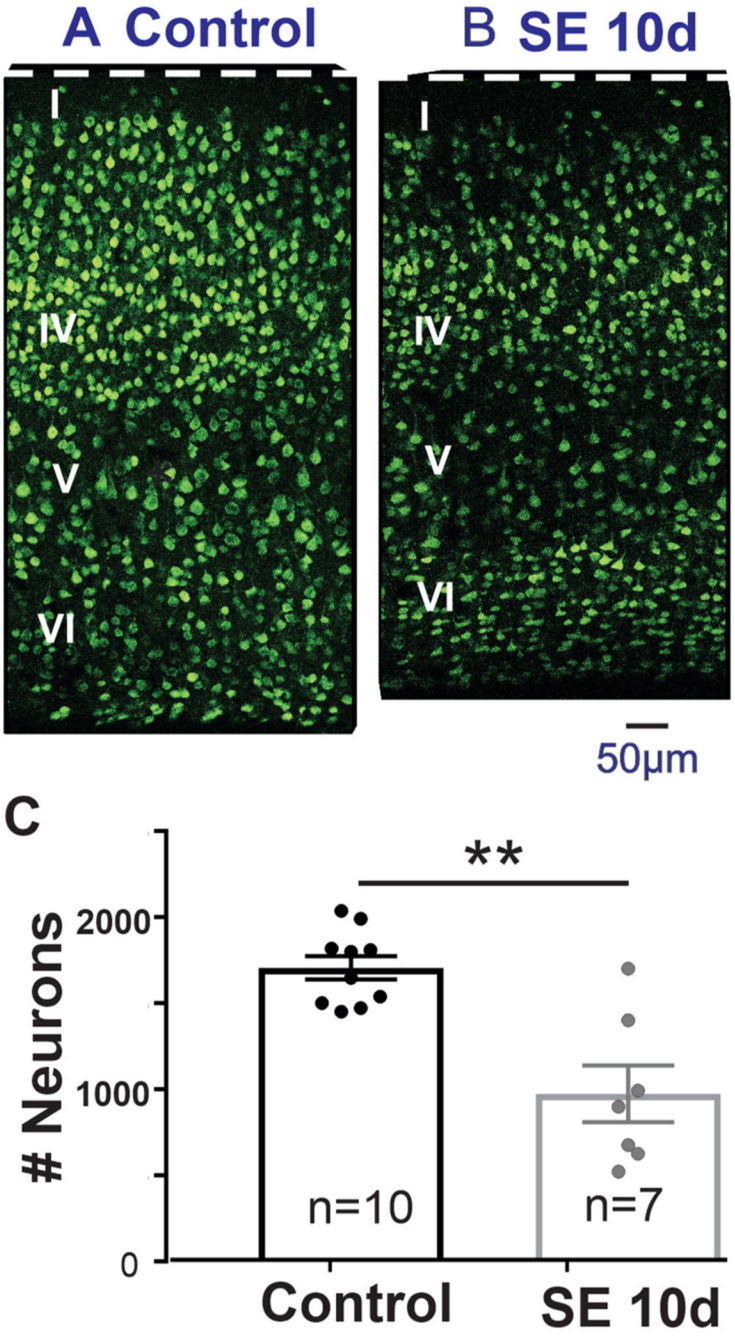

Fig. 2.

Decreased cortical neuronal density and thickness 10d post-FSE. A, B: Confocal images of NeuN-labeled cortical sections of representative control (section A) and 10d post-FSE (section B). Pial surface up (dashed white lines). Approximate centers of layers I, IV-VI marked with Roman numerals. Decreased neuronal density in laminae of B. C: Plot showing the mean number of neurons in the ROI in control (black) and 10d post-FSE (gray). Each dot in plot: Mean number of neurons in one section; n: Number of analyzed sections. **: $p < .01$.

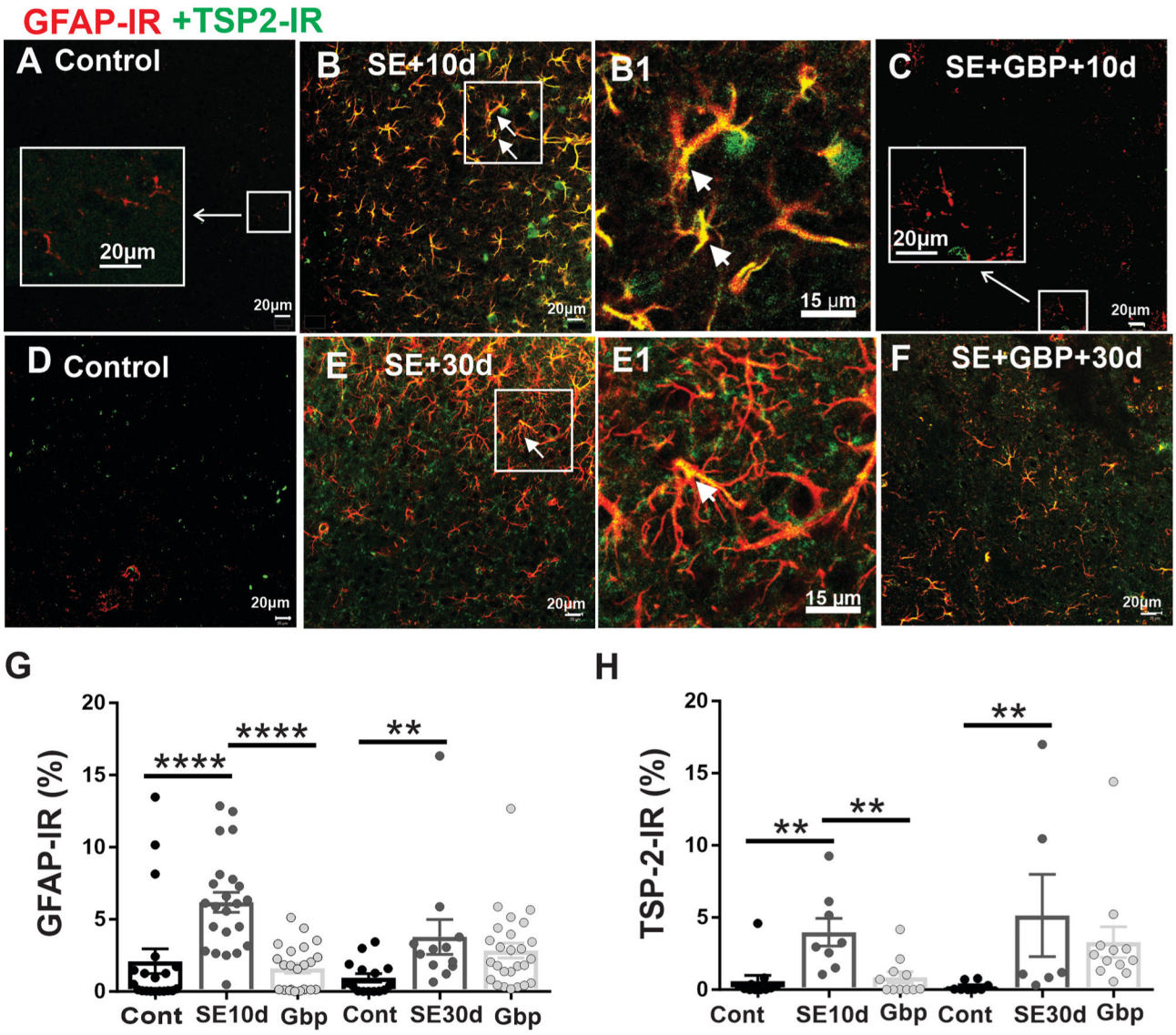

Fig. 3.

GBP treatment (100 mg/kg/day 3× /day × 7 d following FSE) reduces FSE-induced expression of GFAP- and TSP-2-IR. A, D: Control confocal images through layer V of GFAP-IR (red) and TSP-2-IR (green). Area in small white box in A is enlarged with increased brightness and contrast in larger box (arrow) to show GFAP-IR. B, E: Sections showing post-FSE reactive astrogliosis (GFAP) and increased TSP2-IR 10d and 30d post SE. B1, E1: Area within boxes of B and E shown at higher magnification. White arrows: TSP2-IR within reactive astrocytes. C,F: Sections comparable to B and E obtained 10d (C) and 30d post SE (F) in mice treated with GBP for 7d post-SE. Area in small white box in C is enlarged in larger box (arrow) to show GFAP-IR. G,H: Plots showing mean pixel area of GFAP-IR and TSP-2 IR profiles as % of ROI area (200 × 200 μm^2). Each dot in G and H: mean pixel area in one section. **: $p < .01$, ****: $p < .0001$.

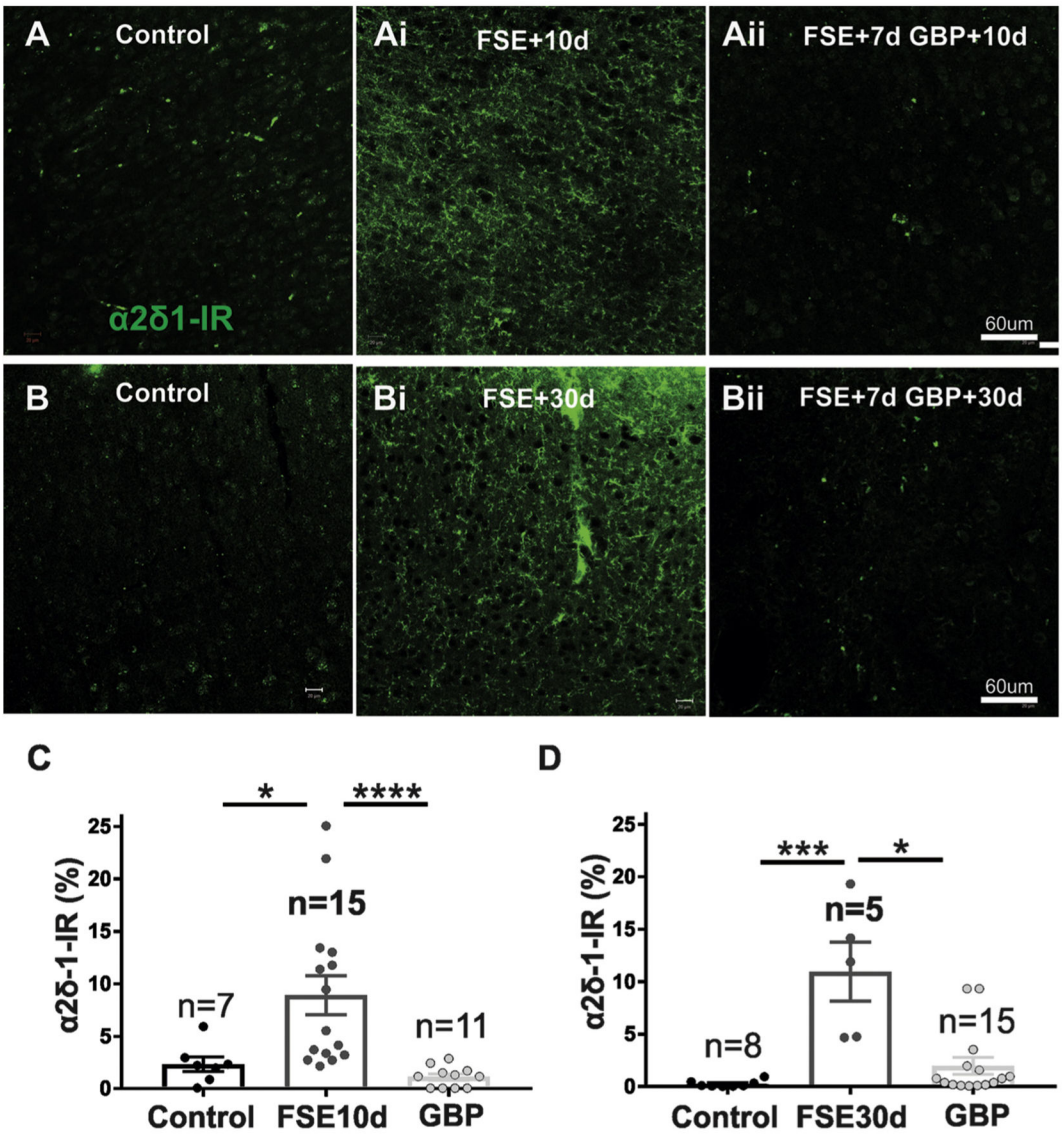

Fig. 4.

Increases in α2δ-1-IR (green) induced by FSE are blocked by GBP treatment. A-B: α2δ-1-IR in confocal images from layer V of control sections. Ai, Bi: α2δ-1-IR in layer V sections 10d and 30d post-FSE. Aii, Bii: α2δ-1-IR 10d and 30d post FSE from layer V in mice treated with GBP × 7d (Methods). C, D: Plots show mean pixel areas of α2δ-1-IR profiles as a % of ROI area (200 × 200 μm^2). *: $p < .1$, ***: $p < .001$, ****: $p < .0001$.

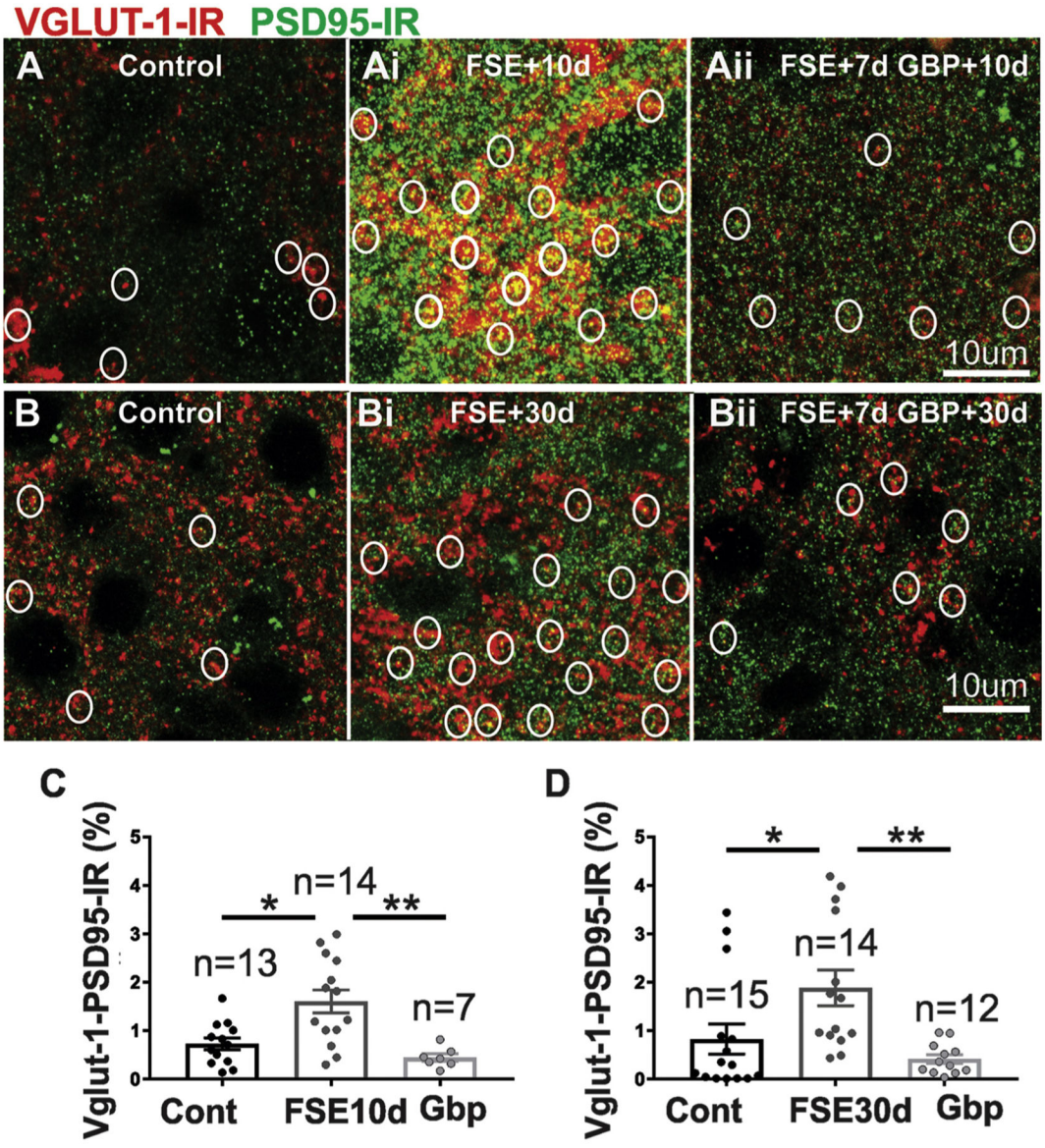

Fig. 5.

Gabapentin reduces post-FSE increases in excitatory synaptic density to control levels. A-B: Control confocal images from cortical layer V showing colocalizations between VGLUT-1- (red) and PSD95-IR (green) (putative excitatory synapses: yellow pixels in white circles). Ai, Bi: Dual VGLUT-1- and PSD95-IR 10d (Ai) and 30d post-FSE (Bi). Aii, Bii: Dual VGLUT-1 and PSP95 10d (Aii) and 30d (Aii) from mice treated with GBP for 7d post-FSE (Methods). C, D: Plots showing mean pixel area of VGLUT-1 and PSD95 colocalization as a % of 40 × 40 μm^2 grids. Each dot: Mean number of neurons in one section; n: Number of analyzed sections. *: $p < .1$, **: $p < .01$.

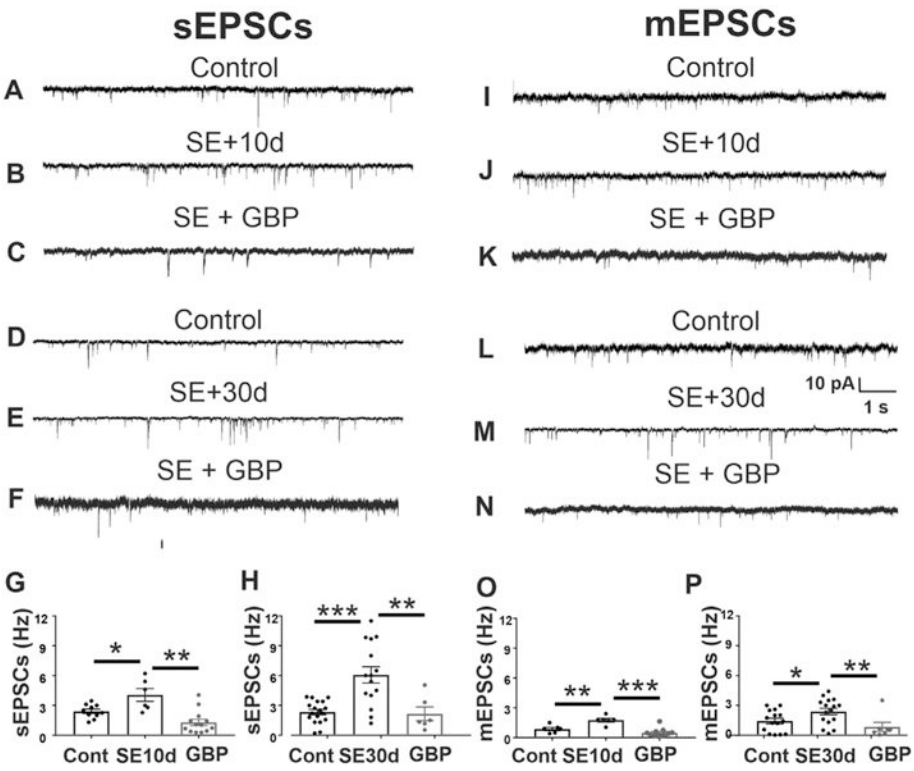

Fig. 6.

FSE-induced increases in frequency of sEPSCs and mEPSCs return to control levels after GBP treatment. A-H: Analysis of sEPSCs. A-C: representative 10s recordings of sEPSCs in control (A), 10 d post-FSE (B), and 10d post-FSE + GBP treatment (C). D- F: As in A, B, C, 30d post-FSE. G: Plots of mean sEPSCs frequency in control, 10d post SE and 10d post SE + GBP treatment. H: As in G 30d + GBP treatment. I-P: Analysis of mEPSCS in TTX (1 μm). I-K: As in A-C, for mEPSCs 10d after FSE. L-N: Representative mEPSCs in control (L), 30d post-FSE (M), and 30d post-FSE + GBP treatment (N). O, P: Plots showing mean mEPSC frequency increases 10 and 30d after FSE. GBP reduced the FSE-induced increases in both sEPSCs and mEPSC frequency to control levels. All recordings from layer V_A in the affected area. Calibrations in L: 10pA, 1 s for all traces; *: $p < .1$, **: $p < .01$, ***: $p < .001$.

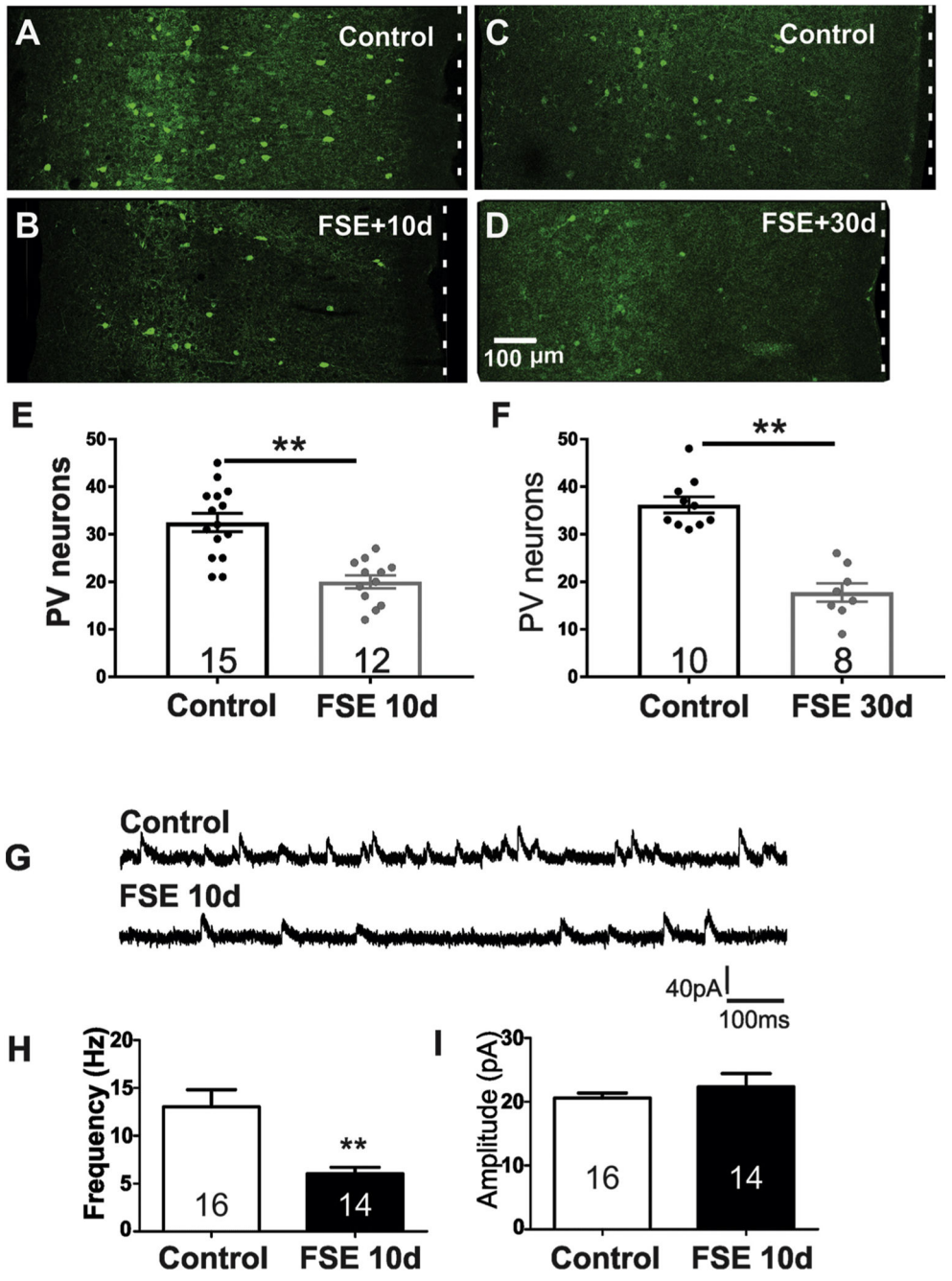

Fig. 7.

Density of PV-containing interneurons is decreased 10 and 30d after FSE. A, C: Confocal images of PV interneurons (green: PV-IR) in all cortical layers in confocal sections from control mice. B, D: Comparable sections through layer V_A 10d (B) and 30d post-FSE (D). Layer VI is on left and pial surface (dashed lines) to right. E, F: Plots showing mean number of PV-IR neurons in control (black), 10 d (E) and 30d post-FSE (gray) (F). G: mIPSCs recorded in TTX from layer V_A of the affected area in control (upper trace) and 10 d post-FSE (lower). H, I: frequency (H) but not the amplitude (I) of mIPSCs was decreased 10 d post-FSE; numbers in bars: number of recorded cells. **: $p < .01$.

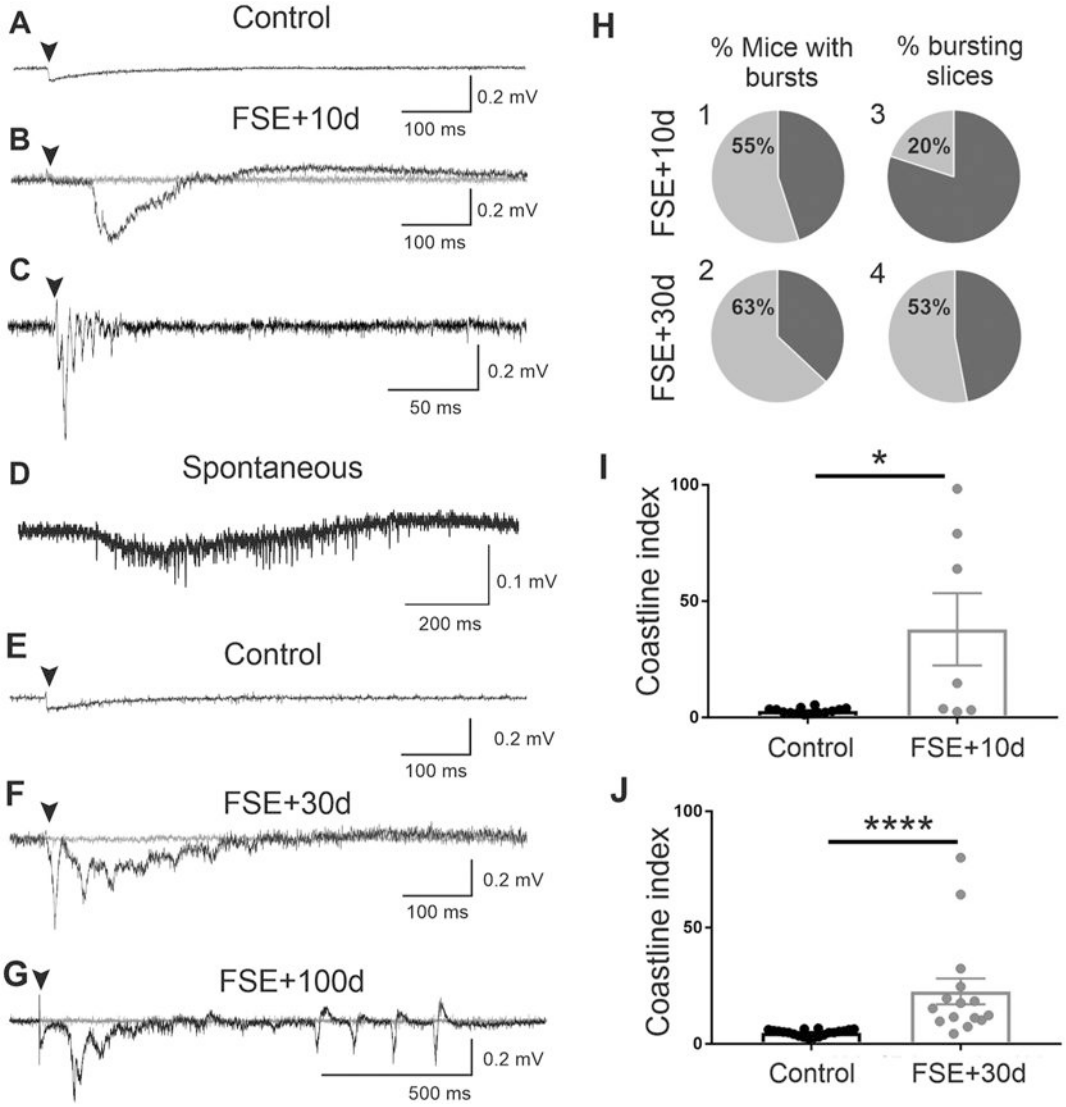

Fig. 8.

Epileptiform local field potential recordings evoked at threshold stimulus intensity after FSE induction. A-G, examples of recordings from layer V in control (A, E), 10d post-FSE (B, C), 30d post-FSE (D, F) and 100d post FSE (G). D, representative spontaneous epileptiform discharge with superimposed unit activity 30d post-FSE. H1,2: % of Mice with bursts: Pie charts showing percentage of all mice recorded in which there was at least one burst-generating slice (gray sector) 10d (H1) and 30d post-FSE (H2). H3–4: percentage of bursting slices in the total number of slices recorded 10 (H3) and 30d post-FSE (H4). I, J: Mean coastline index comparing control (black) and epileptiform potentials (gray) at 10 (I) and 30 d post-FSE (J); *: $p < .1$, ****: $p < .0001$.

Table 1

Results of protein density imaging: mean pixel area as a percentage of ROI in cortical layer V 10 d post-FSE induction, including SEM. Number of analyzed sections is reported in column n. This table is based on 6 mice for control, 6 mice for FSE + saline, and 7 mice for FSE + GBP.

10 days	Control		FSE + saline		FSE + GBP	
	Mean (%)	n	Mean (%)	n	Mean (%)	n
GFAP-IR	2.1 ± 0.8	20	6.2 ± 0.7****	23	1.6 ± 0.3****	23
TSP2-IR	0.6 ± 0.4	11	3.9 ± 0.9**	8	0.8 ± 0.4**	11
α2δ-1-IR	2.3 ± 0.7	7	9 ± 2*	15	1.1 ± 0.3****	11
VGLUT1/PSD95	0.73 ± 0.1	13	1.6 ± 0.2*	14	0.4 ± 0.1**	7

* $P \leq .05$.

** $P \leq .01$.

*** $P \leq .001$.

**** $P \leq .0001$.

Table 2

Results of protein density imaging: mean pixel area as percentage of ROI in cortical layer V 30 d post-FSE induction, including SEM. Number of analyzed sections is reported in column n. This table is based on 7 mice for control, 6 mice for FSE + saline, and 7 mice for FSE + GBP. Asterisks: significance as reported in Table 1; ns = not significant.

30 days	Control		FSE + saline		FSE + GBP	
	Mean (%)	n	Mean (%)	n	Mean (%)	n
GFAP-IR	1 ± 0.3	15	3.8 ± 1.2**	12	2.8 ± 0.5 (ns)	26
TSP2-IR	0.3 ± 0.1	8	5.1 ± 2.8**	6	3.3 ± 1 (ns)	12
α2δ-1-IR	0.2 ± 0.1	8	10.9 ± 3***	5	1.9 ± 0.8*	15
VGLUT1/PSD95	0.9 ± 0.3	15	1.9 ± 0.4*	14	0.4 ± 0.1**	12

Table 3

Mean frequency (black) and amplitude (dark gray) of evoked (s) and mEPSCs, 10 d post FSE. Number of recorded cells is reported in column n. Significance reported on Table 1; ns = not significant.

10 days post-FSE						
Experiment	**Control**		**FSE + saline**		**FSE + GBP**	
	Mean	**n**	**Mean**	**n**	**Mean**	**n**
sEPSCs (Hz)	2.4 ± 0.21	10	4.04 ± 0.6*	6	1.3 ± 0.3**	13
sEPSCs (pA)	10.8 ± 1	10	8.7 ± 1 (ns)	6	11.2 ± 1 (ns)	13
mEPSCs (Hz)	0.9 ± 0.2	6	1.7 ± 0.2**	6	0.5 ± 0.1***	11
mEPSCs (pA)	10.8 ± 1	6	8.7 ± 1 (ns)	6	9.4 ± 1 (ns)	11

Table 4

Mean frequency (black) and amplitude (dark gray) of evoked (s) and mEPSCs, 30 d post FSE. Number of recorded cells is reported in column n. Significance reported on Table 1; ns = not significant.

30 days post-FSE						
Experiment	**Control**		**FSE + saline**		**FSE + GBP**	
	Mean	**n**	**Mean**	**n**	**Mean**	**n**
sEPSCs (Hz)	2.3 ± 0.3	18	6.1 ± 0.9***	15	2.2 ± 0.7**	6
sEPSCs (pA)	9.4 ± 1	18	9.2 ± 0.6 (ns)	15	10.5 ± 1.2 (ns)	6
mEPSCs (Hz)	1.4 ± 0.3	15	2.4 ± 0.3*	16	0.4 ± 0.1**	7
mEPSCs (pA)	8.9 ± 2	15	8.4 ± 1 (ns)	16	10.3 ± 1.3 (ns)	7